Molybdenum angular sputtering distribution under low energy xenon ion bombardment

E. Oyarzabal,[a] J. H. Yu, R. P. Doerner, and G. R. Tynan
Center for Energy Research, University of California at San Diego, La Jolla, California 92093

K. Schmid
Max-Planck Institut für Plasmaphysik, Garching 85748, Germany

(Received 12 December 2005; accepted 19 July 2006; published online 20 September 2006)

The molybdenum angular sputtering distribution is measured during xenon ion bombardment from a plasma, with incident ion energy E_{Xe} ranging between 75 and 225 eV. A quadrupole mass spectrometer (QMS) is used to detect the fraction of sputtered neutrals that is ionized in the plasma and to obtain the angular distribution by changing the angle θ between the target normal and the QMS aperture. The results obtained in these experiments are relative and normalized to the existing data in the literature. The angular sputtering distribution for molybdenum has a maximum at $\theta = 60°$, and this maximum becomes less pronounced as the incident ion energy increases. The dependence of the total sputtering yield on incident ion energy is in good agreement with previous experiments. There is an order of magnitude increase in the sputtering yield as E_{Xe} is increased from 75 to 125 eV, and a more moderate increase for higher energies. The results of a simulation of the angular distribution of molybdenum atoms sputtered by xenon bombardment using a Monte Carlo code are also presented. They are in agreement with the experiments showing an "under-cosine" distribution (peaked at $\theta = 45° - 60°$) for the lower energies which evolves towards a cosine distribution as the incident ion energy increases. © *2006 American Institute of Physics*.
[DOI: 10.1063/1.2336502]

I. INTRODUCTION

Sputtering behavior of ion thruster materials is of great importance in order to model and predict their long term performance. Although the sputtering of various materials has been previously studied in detail for higher incident ion energies,[1–5] there are only a few studies for energies under 200 eV.[6–8] This incident ion energy range is important for the case of sputtering due to low energy ions created by charge exchange reactions near the grid surfaces[9] or by potential hill structures located within ion thruster discharge chambers.[10] Information about the angular sputtering distribution for the thruster materials under these conditions is necessary in order to accurately simulate the net erosion of surfaces and subsequent contamination buildup on adjacent locations.

We present measured angular sputtering distributions of molybdenum (Mo) for low energy normal incident xenon ion bombardment (with incident ion energy E_{Xe} ranging from 75 to 225 eV). A xenon plasma generated in an inductively coupled plasma source is used to provide the singly ionized (due to the low electron temperature T_e) xenon ion flux to the Mo target. The target is negatively biased relative to the plasma to produce the desired bombardment energies, and the sheath that forms in the target surface assures normal incident bombardment. A quadrupole mass spectrometer (QMS) is used to detect the fraction of sputtered neutrals that becomes ionized in the plasma. We use ions as a measure of the fast (few eV) sputtered particle flux because the QMS is several orders of magnitude more sensitive to fast ion detection than to fast neutral detection. The angular sputtering distribution is obtained by changing the relative angle θ between the target normal and the QMS flight path, and these angular distribution measurements are repeated for various incident ion energies. An absolute calibration of the QMS is not possible due to the unknown transmission coefficient for fast Mo ions; thus, the results obtained in these experiments are relative. However, we normalize our data to the existent data from the literature.

A maximum of the angular sputtering distribution at approximately 60° away from the surface normal is observed, which is consistent with previous results that have been reported for low energy high mass bombardment.[7,11,12] Similar results are obtained from simulations performed using the Monte Carlo TRIDYN code.[13] The dependence of the sputtering yield on the incident ion energy is also shown and a comparison with previous data is presented.

II. EXPERIMENTAL SETUP

The schematic of the experimental setup is shown in Fig. 1. The plasma source is an inductively coupled plasma modified from the commercial plasma source M0RI. This source contains magnetic field coils that allow it to operate as a helicon wave plasma source; however, in all of the work reported here these coils are not energized and the source operates in the unmagnetized inductively coupled mode. The source consists of a 100 mm diameter Pyrex bell jar surrounded by a double loop antenna that is driven at a rf of 13.56 MHz. The two antenna loops are 110 mm in diameter

[a]Electronic mail: eoyarzabal@ferp.ucsd.edu

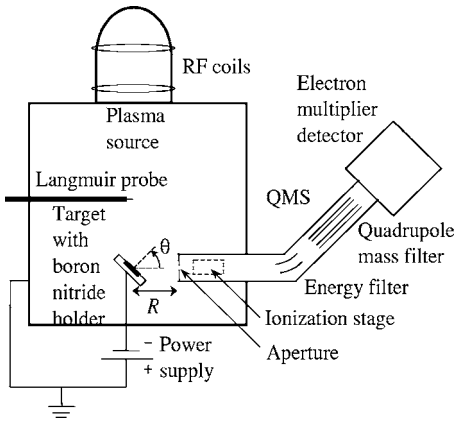

FIG. 1. Schematic of the experimental setup.

and axially spaced 150 mm apart, and are designed such that the rf currents in the two loops are 180° out of phase. The bell jar is attached to a Pyrex bottom plate whose inner and outer diameters are 114 and 166 mm, respectively. This bell jar and plate assembly sits on top of an anodized aluminum reaction chamber, with 350 mm diameter and 400 mm height. A gas injection ring is located on the ceiling of the process chamber at a radius of 93 mm and injects gas into the plasma from four equidistant injection ports. The rf power is coupled to the antenna via a feedback controlled matching network capable of driving the antenna over a wide range of process gases and rf powers. A Langmuir probe is used to measure the electron density and temperature, and is located at the center of the plasma chamber at a distance 16.5 cm below the exit of the plasma source. The sputtered particles are ionized in the plasma and are measured with a QMS (Hiden EQP mass/energy spectrometer). The target and the target holder are mounted at the end of the target manipulator. This manipulator can move the target inside and outside the chamber (so the sample can be changed without venting the entire chamber) and allows the target (together with the target holder) to rotate to a set angle θ between the target normal and the QMS aperture, as can be seen in Fig. 1. The ion bombardment energy is controlled by a negative bias voltage applied to the target. The target holder is made of a nonconducting material and the manipulator is coated with alumina to ensure that only the target is biased. The incident ion flux is calculated from the current collected by the sample and it is found to be independent of the target angle and target bias.

III. SPUTTERING MEASUREMENTS

A QMS, with schematic shown in Fig. 1, is used to analyze the sputtered particles that become ionized in the plasma. Ions enter the QMS through an aperture and are electrostatically energy filtered by passing through a 45° bend in the flight path. These energy-selected ions then enter the quadrupole mass filter, which allows transmission of ions with a desired mass/charge ratio. Finally, the ions arrive at the electron multiplier detector, yielding an ion count rate C_i.

We obtain a rough estimate of the ionization fraction of sputtered particles f_i in terms of the density of ionized sputtered particles in the vicinity of the QMS aperture, n_i,

TABLE I. Experimental parameters.

Pressure (mTorr)	5
rf power (W)	1000
T_e (eV)	2
n_e (cm^{-3})	1×10^{12}
Φ_p (V)	10
Ion flux (ion s^{-1} cm^{-2})	7×10^{16}
A_{QMS} (cm^2)	3×10^{-2}
A_{target} (cm^2)	1.17
R (cm)	10

$$f_i \equiv n_i/n_n = 1 - \exp(-\langle \sigma n_e \rangle R), \tag{1}$$

with

$$\langle \sigma n_e \rangle = n_e \int \sigma(v_e) f_e(v_e) dv_e, \tag{2}$$

where n_n is the sputtered neutral density at the QMS, n_e is the electron density, v_e is the electron velocity, $f_e(v_e)$ is the electron distribution function (assumed here to be Maxwellian), $\sigma(v_e)$ is the electron impact ionization cross section for Mo, and R is the distance from the center of the sample surface to the QMS aperture. In Eq. (2) we assume $v_e \gg v_{Mo}$, where v_{Mo} is the velocity of the Mo atoms, which is true for the range of measured Mo velocities. For the conditions we have in our experiments, shown in Table I, we estimate $f_i \approx 3.2\times10^{-5}$. The fact that we can observe fast ionized sputtered atoms while we cannot see fast neutral sputtered atoms implies that the detection limit for the sputtered Mo neutrals must be at least five orders of magnitude smaller than that for the Mo ions. This large difference in the Mo ion and Mo neutral detection is mainly due to the low efficiency of the QMS ionization stage for the case of fast neutral atom analysis.

The experiments are performed in the following manner: the Mo target is introduced into the chamber at a normal angle with respect to the QMS aperture ($\theta=0°$) and the plasma discharge is started. To make sure the discharge produces the desired plasma parameters (Table I) the density and temperature of the plasma are measured with the Langmuir probe. After the measurement, the probe is move back from the center of the plasma so it does not shadow the sample during the experiments. When the plasma has stabilized, the target is biased to the desired voltage (to achieve the desired xenon ion incident energy) and an energy scan for the sputtered ionized particles is acquired with the QMS. The ions bombard the target surface with an energy given roughly by the difference between the plasma potential (which is monitored with a Langmuir probe) and the bias voltage. The formation of the sheath in the surface of the target assures normal incident ion bombardment, independent of the angle between the target and the QMS aperture. While maintaining the same plasma parameters, the target is biased to the next voltage and another scan is acquired. When the scans for the different incident energies are acquired, the plasma discharge is stopped and the angle between the target and the QMS aperture is changed. We repeat the process described above for all the angles studied. The

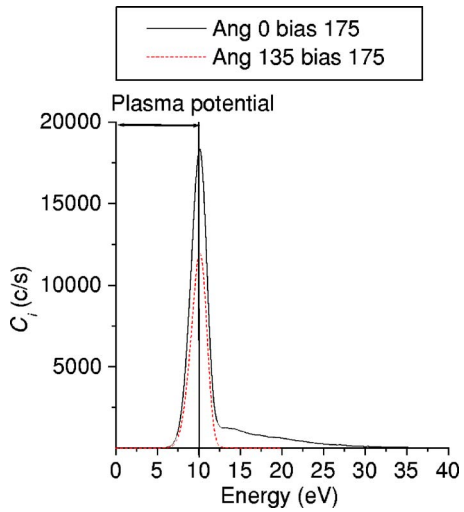

FIG. 2. Mass 98 ion count rate vs energy for Mo sputtering under xenon bombardment.

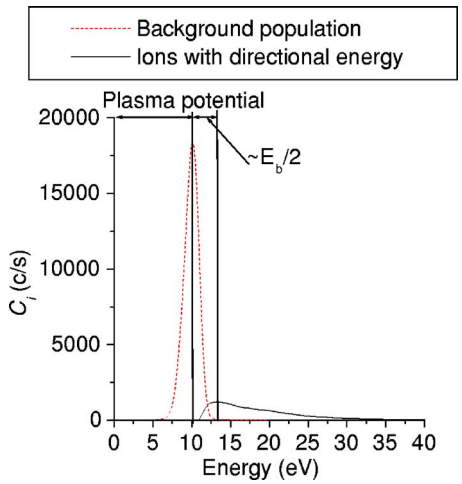

FIG. 3. Background population and population of the particles with directional energy vs energy for Mo sputtering under xenon bombardment.

acquired energy distributions are integrated to obtain the angular sputtering for the different incident ion energies, as explained below.

IV. DATA ANALYSIS

Figure 2 shows the QMS ion count rate C_i versus energy for mass 98 ions (Mo). The observed energy distribution can be interpreted using some basic plasma surface interaction behavior. Due to the formation of a sheath at the QMS wall, which is grounded, ions are accelerated before entering the QMS. The energy that the ions gain in going through this sheath region is equal to the plasma potential Φ_p. This potential energy must be subtracted from the energy scale of the raw data to obtain the actual energy scale of the ion energy distribution in the plasma.

Figure 2 shows that even when the sample is not facing the QMS, i.e., when the sample normal is set at an angle of 135° with respect to the QMS flight path, we still detect a finite ion signal for Mo. We believe that this background signal is due to collisions with neutrals in the plasma. Mo sputtered atoms that undergo elastic scattering lose their directional energy and are driven toward thermal equilibrium with the xenon neutrals. The fraction of these near-thermal Mo atoms that is ionized afterwards in the plasma accounts for the measured ion signal at angle $\theta=135°$; we call this ion population the "background population."

These collisions with neutrals affect the energy distribution of the particles with directional energy. Since the sputtered Mo atom mass is close to that of the working gas (xenon) and plasma ion, a single elastic scattering event of a fast (few eV) Mo atom with a thermal (0.1 eV or less) xenon scattering center will result in a significant transfer of energy from the fast species to the slower species. Consider an initial sputtered particle energy distribution $f_0(E)$ at a particular sputtering angle. Mo-xenon scattering changes this energy distribution with distance R from the sample as

$$f(E,R) = f_0(E)\exp(-\sigma_{\text{Mo–Xe}} n_n R), \tag{3}$$

where $\sigma_{\text{Mo–Xe}}$ is the Mo-xenon scattering cross section and n_n is the neutral density. We neglect collisions with plasma ions here because the neutral density is at least two orders of magnitude higher than the plasma ion density for the conditions in our experiments. Essentially, the distribution function of the ions measured at a certain distance from the sample is a constant fraction of the original neutral sputtered particle distribution because $\sigma_{\text{Mo–Xe}}$ does not depend on the energy of the sputtered particles.[14] Thus, the measured ion energy spectra (with the background population subtracted) directly represents attenuated sputtered neutral particle energy spectra.

In order to measure the angular distribution of the sputtered Mo, we subtract the background population of ions (which does not keep any directional information) from the raw data and obtain the count rate of the ion population with directional energy. The background population for each experimental condition is obtained by normalizing the peak value of the signal at $\theta=135°$ to the peak value of the signal for that particular experimental condition. Figure 3 shows the background population distribution normalized according to the procedure described above and the resulting distribution of the particles with directional energy after the background subtraction in the case of $\theta=0°$ and $E_{\text{Xe}}=175$ eV. The energy difference between the peaks of these two populations corresponds to roughly half of the surface binding energy for Mo ($E_b \approx 6.9$ eV). This directed energy distribution of fast particles is then summed over the whole energy range to obtain a total ion signal $S_i \equiv \Sigma C_i(E)$ for each experimental condition.

We verify that the elastic scattering of Mo off xenon neutrals is the dominant collision mechanism by performing an experiment in which the Mo ion signal is acquired for different neutral gas pressures (P). The other parameters of the plasma and the experiment are nearly constant (less than 10% change) in the pressure range selected (10–21 mTorr), so the change in the ion signal is only due to the change in the neutral density (neutral temperature is nearly constant as well). Figure 4 shows the measured Mo ion signal S_i versus the pressure and shows a fit to an exponentially decaying

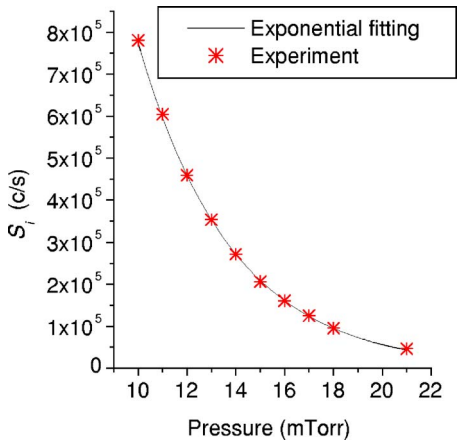

FIG. 4. Ion signal S_i vs pressure and fitting of the exponentially decaying signal of the elastic scattering process.

signal that corresponds to an elastic scattering process, $C\exp(-\sigma_{\mathrm{Mo-Xe}}n_nR)$, where C and $\sigma_{\mathrm{Mo-Xe}}$ are the fitting parameters. The neutral density is obtained from the ideal gas law, $n_n=P/kT$, where the temperature (T) of the neutral xenon particles is measured spectroscopically as explained in Ref. 15, and has a value of 650 K. The fit describes the data extremely well and predicts a Mo-xenon cross section $\sigma_{\mathrm{Mo-Xe}}=1.85\times10^{-15}$ cm^2, which is in very good agreement with the theoretical cross section for Mo-xenon collisions assuming hard sphere collisions, $\sigma_{\mathrm{theor}}=\pi(R_{\mathrm{Xe}}+R_{\mathrm{Mo}})^2=1.91\times10^{-15}$ cm^2 (where $R_{\mathrm{Xe}}=1.08\times10^{-8}$ cm is the xenon atomic radii and $R_{\mathrm{Mo}}=1.39\times10^{-8}$ cm is the Mo atomic radii). Thus, elastic collisions of sputtered fast Mo atoms with the background neutral xenon atoms in the plasma are responsible for the background population peak we observe in the energy distribution of Mo, and the signal S_i does, in fact, represent the flux of uninteracted Mo particles that have maintained their original directional energy.

Finally, the ion signal S_i is normalized so that the total sputtering yield for 150 eV incident energy is the same as in previous low energy normal incidence xenon on Mo bombardment literature data.[17] In this way, we obtain a differential sputtering yield for each observation angle at each incident energy.

V. RESULTS AND DISCUSSION

A. Angular distribution of the sputtered Mo particles

Figure 5 shows the polar plots of the obtained angular sputtering distributions of Mo under xenon bombardment for various incident ion energies. The data have been plotted as a mirror image around $\theta=0°$ to make the figures easier to visualize. For all the incident energies studied in this work, the sputtering yield is "under cosine," with a maximum at an angle of 60°. This maximum is less pronounced as the incident energy increases. Similar under-cosine angular sputtering distributions have been reported previously during low energy bombardment for the case of high mass ratio between the incident ion and the target material.[7,11,12]

Simulation of the angular distribution of Mo atoms sputtered by xenon bombardment using the Monte Carlo code TRIDYN (Ref. 13) predicts similar results, as can be seen in

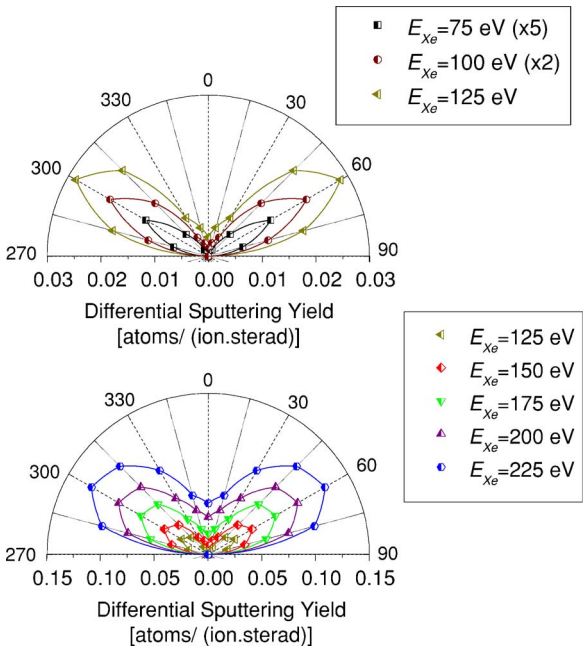

FIG. 5. Mo angular sputtering distribution for incident ion energies from 75 to 125 eV (upper plot) and from 125 to 225 eV (lower plot). Data for 75 and 125 eV have been multiplied by 5 and 2, respectively. Data are mirrored around 0° for clarity.

the polar plot in Fig. 6. The code models the transport of incident energetic particles and generated recoils in an amorphous target as a sequence of independent binary collisions. The Krypton-C interaction potential[13] is used to describe the scattering processes within this collision cascade. When a Mo atom from the cascade leaves the surface with energy larger than the surface binding energy, it is considered sputtered, and its exit angle relative to the surface normal is recorded. From the relative sputter yield of particles sputtered into a certain angle, the angular distribution $P(\theta)$ is calculated according to

$$2P(\theta)=[1/Y(E_{\mathrm{Xe}})][dY(E_{\mathrm{Xe}})/d\cos(\theta)]. \tag{4}$$

The results of the simulation show an under-cosine distribution with a maximum at around 45° for the lower energies (<500 eV) and a cosinelike distribution for the higher energies (500 and 1000 eV). The results of the simulation are not in complete agreement with the experiments, which show a more pronounced maximum at 60° (instead of 45°) for both

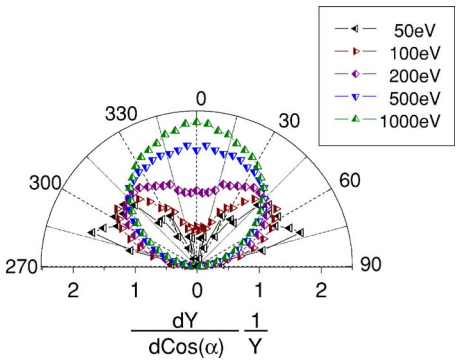

FIG. 6. Simulated Mo angular sputtering distribution for different incident ion energies. Data are mirrored around 0° for clarity.

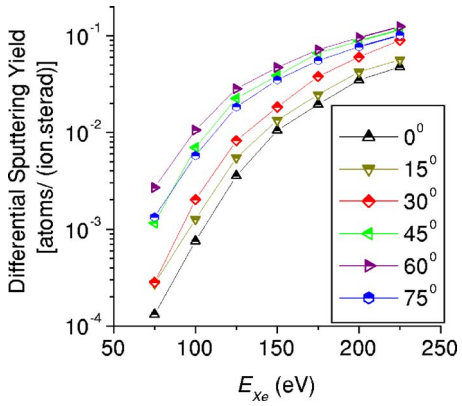

FIG. 7. Mo differential sputtering yield vs incident ion energy for different sputtering angles.

100 and 200 eV incident energies. Nevertheless, both the simulation and the experimental results present a similar evolution of the angular distribution with the incident energy, showing an under-cosine angular sputtering distribution when the kinetic energy of the heavy ions is too small to create collisional cascades, resulting in a decrease of sputtered particles ejected normal to the surface.[16] For much larger incident energies the simulated sputtering angular distribution evolves toward the well-known cosine distribution.

B. Mo sputtering versus incident energy

The differential sputtering yield versus incident energy for various observation angles is shown in Fig. 7. The dependence of the sputtering on the incident energy is similar for the different sputtering angles. There is a large increase of an order of magnitude in the sputtering yield from $E_{\mathrm{Xe}}=75$ to 125 eV, and a more moderate increase for higher energies.

The dependence of the total sputtering yield on the incident ion energy is in good agreement with previous experiments, as can be seen in Fig. 8. This result gives us confidence in the validity of our experimental procedure to correctly measure the sputtering behavior of the studied material. The sputtering yield at higher energies in Ref. 6 appears to be somewhat smaller than that in the other studies. We believe that the reason for this disagreement is likely due to the fact that the results of Ref. 6 were calculated by assuming a cosine distribution of the sputtered particles. We believe that the present data can be used to estimate the magnitude of the correction necessary for the data in Ref. 6, but such calculations will require both angular and sputtered particle energy corrections and are outside the scope of this paper. The corrections will be treated in a separate publication.

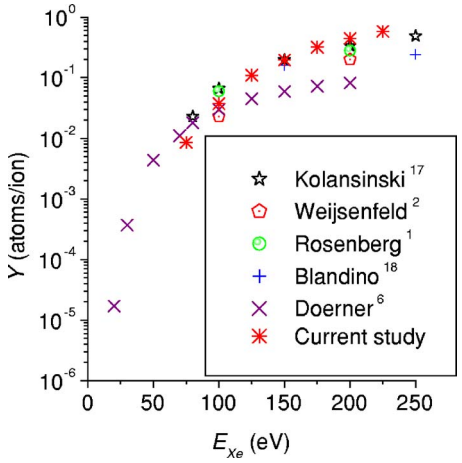

FIG. 8. Comparison of the total sputtering yield vs incident ion energy with previous experiments.

VI. CONCLUSIONS

The Mo angular sputtering distribution during low energy (75–225 eV) normal incidence xenon ion bombardment has been measured using a quadrupole mass spectrometer (QMS) to detect the fraction of sputtered neutrals that is ionized in the plasma. The results obtained in these experiments are relative and have been normalized to the existing data in the literature.

An "under-cosine" angular sputtering distribution of Mo with a maximum at around 60° for the studied xenon incident ion energy range (75–225 eV) is observed. This maximum becomes less pronounced as the incident energy increases. These kind of under-cosine angular distributions, with maximum at approximately $\theta=60°$, have been reported previously during low energy sputtering experiments.[7,11,12] We observe the same angular distribution evolution with incident energy in the simulations performed using the Monte Carlo TRIDYN code. For low incident ion energy bombardment (<500 eV) the kinetic energy of the ions is too small to create collisional cascades, resulting in a decrease of sputtered particles ejected normal to the surface.[17] For larger incident energies, the simulated sputtering angular distribution evolves toward the well-known cosine distribution.

Comparison of the total sputtering yield results of Mo with previous experiments shows good agreement. There is a large increase of about an order of magnitude in the sputtering yield from $E_{\mathrm{Xe}}=75$ to 125 eV, and a more moderate increase for higher energies. This result gives us confidence in the validity of our experimental procedure to correctly measure the sputtering behavior of the studied material.

The measurements presented here show that the typically assumed cosine distribution of sputtered particles during low energy, high mass ion bombardment of surfaces may not be valid. The angular distribution of sputtered particles will to a large extent determine the locations where redeposited material may accumulate in ion thruster engines.

ACKNOWLEDGMENTS

This work was supported by NASA through the Jet Propulsion Laboratory/Caltech. The authors would like to thank Tyler Lynch for his continuous technical support and Kurt Taylor, Masashi Shimada, and Jeremy Hanna for their help while performing the experiments.

[1] D. Rosenberg and G. K. Wehner, J. Appl. Phys. **33**, 1842 (1962).
[2] C. H. Weijsenfeld, A. Hoogendoorn, and M. Koedam, Physica (Amsterdam) **27**, 763 (1961).
[3] P. C. Zalm, J. Appl. Phys. **54**, 2660 (1983).

[4]M. A. Mantenieks, P. K. Ray, and S. V. Shutthanandan, *Proceedings of the International Electronic Propulsion Conference*, Pasadena, CA, 15–19 October 2001 (unpublished), Paper No. IEPC-309.
[5]J. D. Williams, M. L. Johnson, and D. D. Williams, AIAA Paper No. 2004-3788, 2004 (unpublished).
[6]R. P. Doerner, D. G. Whyte, and D. M. Goebel, J. Appl. Phys. **93**, 5816 (2003).
[7]M. N. Nakles, J. Pierru, J. J. Wang, S. V. Shutthanandan, Y. Zang, and W. R. Wiley, AIAA Paper No. 2003-5160, 2003 (unpublished).
[8]R. Kolansinski, AIAA Paper No. 2004-4110, 2004 (unpublished).
[9]C. C. Farnell, J. D. Williams, and P. J. Wilbur, *Proceedings of the International Electric Propulsion Conference*, Toulouse, France, 17–21 March 2003 (unpublished), Paper No. IEPC-03-073.
[10]J. E. Foster and M. J. Patterson, AIAA Paper No. 2002-4102, 2002 (unpublished).
[11]D. Rosenberg and G. K. Wehner, J. Appl. Phys. **31**, 177 (1960).
[12]J. D. Williams, M. M. Gardner, M. L. Johnson, and P. J. Wilbur, National Aeronautics and Space Administration, Report No. NASA-CR-2003-212306, 2003 (unpublished).
[13]W. Möller, W. Eckstein, and J. P. Biersack, Comput. Phys. Commun. **51**, 355 (1988).
[14]G. V. Walter and H. K. Charles, *Introduction to Physical Gas Dynamics* (Krieger, Malabar, FL, 1986), p. 14).
[15]M. Shimada, J. Vac. Sci. Technol. A (to be published).
[16]T. Okutani, M. Shikata, S. Ichimura, and R. Shimizu, J. Appl. Phys. **51**, 2884 (1980).
[17]R. Kolansinski, AIAA Paper No. 2005-3526, 2005 (unpublished).
[18]J. J. Blandino, D. G. Goodwin and C. E. Garner, Diamond Relat. Mater. **9**, 1992 (2000).